Physica D 481 (2025) 134865

Contents lists available at ScienceDirect

Physica D

journal homepage: www.elsevier.com/locate/physd

Learning dissipation and instability fields from chaotic dynamics

Ludovico T. Giorgini [a,*], Andre N. Souza [b], Domenico Lippolis [c], Predrag Cvitanović [d], Peter Schmid [e]

[a] Department of Mathematics, MIT, Cambridge, MA, USA
[b] Department of Earth, Atmospheric, and Planetary Sciences, MIT, Cambridge, MA, USA
[c] Department of Physics, Tokyo Metropolitan University, Hachioji, 192-0397, Japan
[d] Center for Nonlinear Science, School of Physics, Georgia Institute of Technology, Atlanta, 30332-0430, GA, USA
[e] Physical Science and Engineering Division, KAUST, Thuwal, 23955-6900, Saudi Arabia

ARTICLE INFO

Communicated by Stephen Wiggins

Keywords:
Chaotic dynamics
Data-driven modeling
State-space partition
Jacobian
Perron–Frobenius
Koopman

ABSTRACT

This paper establishes a novel theoretical connection between the operator-theoretic description of a dynamical system and its local geometric properties. We demonstrate that the local Jacobian determinant, which governs state-space expansion and contraction, can be directly related to the entries of the transition matrix that approximates the system's Perron–Frobenius operator. Specifically, we derive expressions that link measures of local instability and dissipation to the matrix elements, revealing that these geometric features are intrinsically encoded in the statistical operator. We illustrate the validity of this relationship through numerical experiments on several one- and two-dimensional chaotic maps, where these derived measures are validated against the exact analytical Jacobians of these test systems. This work establishes a direct, quantitative link between the global, statistical view of dynamics provided by the Perron–Frobenius operator and the local, geometric perspective described by the Jacobian.

1. Introduction

The challenge of characterizing a dynamical system from observed data is fundamental across theoretical and applied physics. This endeavor is not only academically significant but also has practical implications in diverse scientific disciplines, where understanding the underlying mechanisms of observed phenomena is paramount [1]. Even if the dynamical systems under consideration are exceedingly high-dimensional, making an accurate description of the interactions between all scales and variables unfeasible, low-order representations can often be constructed to retain the most important statistical and dynamical features of the system, effectively capturing the essential behavior without the need for exhaustive detail [2–5]. These simplified models provide a practical means of analyzing core dynamics and allow for meaningful analysis and prediction, even in complex, high-dimensional contexts [6–11].

Reduced-order models play a crucial role, for example, in climate physics by effectively describing interacting degrees of freedom and capturing key feedback mechanisms across spatial and temporal scales [12–22]. In finance, reduced-order models are used to understand market dynamics and to develop robust economic models, such as the Black–Scholes model [23], a key tool in financial mathematics. In biology, particularly in the study of ecosystems, disease propagation, and epidemiology, reduced-order models like the Lotka–Volterra equations provide insights into complex interactions, such as predator–prey dynamics [24]. The success of these approaches often hinges on their ability to capture not just trajectories, but also fundamental properties like long-term statistical distributions and local measures of stability.

Despite remarkable success, reconstructing low-order models from observed data becomes particularly challenging in highly nonlinear and chaotic systems, where the inherent complexity and sensitivity to initial conditions make it difficult to accurately capture the essential dynamics using simplified models [25–27]. Nonetheless, although a precise mathematical model driving observed data remains elusive, the statistical features of the dynamical system can often be robustly estimated from data, provided a statistically significant amount of observations is available [22,28–35].

A classical data-driven approach to estimate local dynamics and their derivatives, such as the Jacobian, involves identifying k-nearest neighbors (k-nn) to a point in the state space and then performing a local regression. This method, rooted in the early days of chaos

* Corresponding author.
E-mail addresses: ludogio@mit.edu (L.T. Giorgini), sandre@mit.edu (A.N. Souza), lippolis@tmu.ac.jp (D. Lippolis), predrag.cvitanovic@physics.gatech.edu (P. Cvitanović), peter.schmid@kaust.edu.sa (P. Schmid).
URLs: https://ludogiorgi.github.io (L.T. Giorgini), https://sandreza.github.io (A.N. Souza), https://ChaosBook.org (P. Cvitanović).

https://doi.org/10.1016/j.physd.2025.134865
Received 5 February 2025; Received in revised form 23 July 2025; Accepted 27 July 2025
Available online 5 August 2025

theory, leverages the idea that the evolution of nearby points can be approximated by a linear map, representing the local tangent map or its derivative, the Jacobian [36]. By collecting a set of neighbors for a point $\boldsymbol{x}(i)$, one can use their subsequent states $\boldsymbol{x}(j+1)$ to fit a linear model that estimates the Jacobian matrix. This is often achieved through a least-squares fit of the differences $\boldsymbol{x}(j+1)-\boldsymbol{x}(i+1)$ against $\boldsymbol{x}(j)-\boldsymbol{x}(i)$. The number of neighbors, k, acts as a smoothing parameter: a larger k increases robustness to noise but introduces bias by averaging over a larger region, while a smaller k offers higher accuracy in smooth regions but is more sensitive to noise. This direct regression approach has been a cornerstone for forecasting and controlling chaotic systems for decades [37–39].

In this paper, we establish and investigate a novel connection between the global statistical properties of a dynamical system and its local geometric features. We demonstrate that information about the Jacobian determinant is intrinsically encoded within the transition matrix that approximates the Perron–Frobenius operator. This operator describes how a probability density of states evolves in time and is the adjoint to the more widely known Koopman operator [40,41]. By assuming a Markovian process on a partitioned state space, the infinite-dimensional Perron–Frobenius operator can be approximated by a finite transition matrix learned directly from observed data [42–44]. Our work shows how this standard operator-based perspective, already effective in fields like network science [45] and computational neuroscience [46], can be leveraged to extract valuable local dynamical information as an intrinsic by-product of the construction of the Perron–Frobenius operator.

The Jacobian determinant is a fundamental quantity describing local stretching, contraction, and dissipation. We show that the connection between the transition matrix and the system's dynamics allows for the derivation of two data-driven observables which provide bounds on local dissipation and instability rates. This offers a unique means of probing the Jacobian without direct regression, offering insight into the underlying dynamics from purely statistical information. This approach bridges the gap between statistical descriptions of dynamics and the local geometric properties of the flow.

We focus here on discrete-time dynamical systems of form $\boldsymbol{x}^{n+1} = \boldsymbol{f}(\boldsymbol{x}^n)$, where $n \in \mathbb{N}$ is the nth discrete time step, $\boldsymbol{x} = \{x_1, \dots, x_D\}$ is a D-dimensional vector representing the state of the system, and $\boldsymbol{f} : \mathbb{R}^D \to \mathbb{R}^D$ is the forward map that characterizes the evolution of the system in time. For non-autonomous dynamical systems, we augment the dimension of the state vector, in order to incorporating external time-dependent changes.

The key observation to connect the dynamics with the Jacobian is that a density of trajectories at time n, $\rho^n(\boldsymbol{x})$, is transformed by the Perron–Frobenius operator as [47]

$$\rho^{n+1}(\boldsymbol{x}) = \sum_{k=1}^{M} \frac{\rho^n(\boldsymbol{f}_k^{-1}(\boldsymbol{x}))}{|J(\boldsymbol{f}_k^{-1}(\boldsymbol{x}))|}\,.$$

As explained below, in the evolution of a density by the Perron–Frobenius operator (our means), which is in general a contraction [48], one can identify the local dissipation with the Jacobian J of the map (our goal), computed on the M preimages $\boldsymbol{f}_k^{-1}(\boldsymbol{x})$. We shall show that a lower bound for the local Jacobian $J(\boldsymbol{x})$ may also be estimated from the entries of the transfer matrix (in one dimension, $J(\boldsymbol{x})$ is the derivative of the map). The transfer matrix can be constructed directly from observed data, and hence the Jacobian determinant can also be estimated without knowing the system's governing equations. The methodology proposed here is therefore data driven.

Knowledge of dissipation and of instability fields is essential for analysis, forecast, and control. In particular, potential applications of our methodology include stabilizing an unstable system [49], enhancing the sensitivity to initial conditions in chaotic systems [50], or ensuring that conservation laws are adhered to in physical models [51,52], when direct evaluation of the Jacobians is unavailable due to computational challenges, or ignorance of the governing equations, as in experimental time series. This knowledge is invaluable not only for understanding of the intrinsic properties of the system, but also in facilitating the design of more effective and controlled dynamical models. This paper aims to demonstrate the utility of this approach through a detailed theoretical analysis and application to simulated data, highlighting its potential impact across a broad spectrum of scientific disciplines.

The article is structured as follows. Section 2 explains how the Jacobian of the map can be inferred from the transition matrix, in Section 3 we apply this methodology to one- and two-dimensional chaotic maps, and Section 4 presents our conclusions.

2. From the transition matrix to the Jacobian

The *Perron–Frobenius operator* $\mathcal{P}$ encapsulates how a probability density function $\rho^n(\boldsymbol{x})$ at time step n evolves under the flow induced by the forward map $\boldsymbol{f}$,

$$\rho^{n+1}(\boldsymbol{x}) \;=\; \big(\mathcal{P}\rho^n\big)(\boldsymbol{x})\,.$$

To construct a *discrete* approximation of this operator, we partition the state space into N equally sized *control volumes*,

$$\boldsymbol{X} = [\boldsymbol{X}_1, \dots, \boldsymbol{X}_N]\,. \tag{1}$$

Each control volume has measure

$$\mu(\boldsymbol{X}_i) \;=\; \frac{\Omega}{N},$$

where Ω is the total volume of the explored region. We denote the probability mass in each control volume at time n by

$$q_i^n \;=\; \int_{\boldsymbol{X}_i} \rho^n(\boldsymbol{x})\, d\boldsymbol{x}.$$

Since $\mathcal{P}$ acts linearly on ρ^n, its discretization is a time-independent *transition matrix* $\boldsymbol{P} \equiv (P_{ij})$ that evolves the discretized state-space vector $\{q_j^n\}_{j=1}^N$ to $\{q_i^{n+1}\}_{i=1}^N$ according to

$$q_i^{n+1} \;=\; \sum_{j=1}^{N} P_{ij}\, q_j^n. \tag{2}$$

By construction, the transition matrix $\boldsymbol{P}$ satisfies:

$$\sum_{i=1}^{N} P_{ij} \;=\; 1 \quad \text{for each } j.$$

Moreover, since P_{ij} represents the probability of transition from cluster j to cluster i, it also holds that

$$0 \;\le\; P_{ij} \;\le\; 1. \tag{3}$$

When each control volume $\boldsymbol{X}_j$ is mapped forward by the underlying flow, the probability mass is reallocated to possibly multiple volumes $\boldsymbol{X}_i$. Thus, the entries of $\boldsymbol{P}$ encode the local stretching or contraction of volumes under the flow map, which is directly linked to the *Jacobian* of the forward map $\boldsymbol{f}$. As we refine the partition the transition matrix $\boldsymbol{P}$ approaches the action of the continuous Perron–Frobenius operator, and each transition P_{ij} may be interpreted as a (coarse-grained) representation of volume expansion/contraction governed by the Jacobian. We present next an explicit derivation of how these matrix elements relate to the underlying Jacobian structure of the dynamical system.

Following Refs. [26,53], we have

$$\rho^{n+1}(\boldsymbol{x}) = \int_{\boldsymbol{X}} d\boldsymbol{y}\, \delta(\boldsymbol{x}-\boldsymbol{f}(\boldsymbol{y}))\rho^n(\boldsymbol{y}) = \sum_{k=1}^{M} \frac{\rho^n(\boldsymbol{f}_k^{-1}(\boldsymbol{x}))}{|J(\boldsymbol{f}_k^{-1}(\boldsymbol{x}))|},$$

for each $\boldsymbol{x} \in \Omega$, where $\boldsymbol{f}_k^{-1}$ denotes the $k \in \{1, \dots, M\}$ preimages of the forward map $\boldsymbol{f}(\boldsymbol{x})$, and J is the Jacobian of the transformation. Integrating both sides of the equation in state space over the cluster $\boldsymbol{X}_i$ yields

$$q_i^{n+1} = \int_{\boldsymbol{X}_i} \rho^{n+1}(\boldsymbol{x})\; d\boldsymbol{x} = \int_{\boldsymbol{X}_i} \sum_{k=1}^{M} \frac{\rho^n(\boldsymbol{f}_k^{-1}(\boldsymbol{x}))}{|J(\boldsymbol{f}_k^{-1}(\boldsymbol{x}))|}\; d\boldsymbol{x}. \tag{4}$$

Now suppose that the partition $\boldsymbol{X}$ is sufficiently fine, and that the Jacobian is sufficiently smooth, so that in the integral of Eq. (4) it can be approximated by its value at the centroid $\boldsymbol{C}_i$ of $\boldsymbol{X}_i$. Under these assumptions, we obtain

$$\begin{aligned} q_i^{n+1} &\approx \sum_{k=1}^{M} \frac{1}{\left|J\left(\boldsymbol{f}_k^{-1}(\boldsymbol{C}_i)\right)\right|} \int_{\boldsymbol{X}_i} \rho^n\left(\boldsymbol{f}_k^{-1}(\boldsymbol{x})\right)\, d\boldsymbol{x} \\ &= \sum_{k=1}^{M} \frac{1}{\left|J\left(\boldsymbol{f}_k^{-1}(\boldsymbol{C}_i)\right)\right|} \sum_{j=1}^{N} p_{ij}^k\, q_j^n, \end{aligned} \tag{5}$$

where in the second step we have defined

$$\sum_{j=1}^{N} p_{ij}^k\, q_j^n \;:=\; \int_{\boldsymbol{X}_i} \rho^n\left(\boldsymbol{f}_k^{-1}(\boldsymbol{x})\right)\, d\boldsymbol{x}\,.$$

The coefficients p_{ij}^k are the elements of a non-negative matrix representing the Koopman operator (the adjoint of the Perron–Frobenius operator) of $\boldsymbol{f}_k^{-1}$

$$\rho^n\left(\boldsymbol{f}_k^{-1}(\boldsymbol{x})\right) = \int_{\boldsymbol{X}} d\boldsymbol{y}\, \delta(\boldsymbol{y} - \boldsymbol{f}_k^{-1}(\boldsymbol{x}))\rho^{n+1}(\boldsymbol{y})\,,$$

on a discretized state space. The Koopman operator evolves the probability densities *backward* in time through the inverse map $\boldsymbol{f}_k^{-1}$. Concretely, each p_{ij}^k encodes the probability that the kth preimage of the ith cluster centroid, i.e. $\boldsymbol{f}_k^{-1}(\boldsymbol{C}_i)$, lies in cluster $\boldsymbol{X}_j$. In addition, the p_{ij}^k obey the normalization conditions and bounds:

$$\sum_{j=1}^{N} p_{ij}^k \;=\; 1 \quad \text{for all } i,k, \tag{6}$$

$$0 \;\le\; p_{ij}^k \;\le\; 1 \quad \text{for all } i,j,k. \tag{7}$$

Rewriting Eq. (5) as

$$\begin{aligned} q_i^{n+1} &\approx \sum_{k=1}^{M} \frac{1}{|J(\boldsymbol{f}_k^{-1}(\boldsymbol{C}_i))|} \sum_{j=1}^{N} p_{ij}^k q_j^n \\ &= \sum_{j=1}^{N} \left(\sum_{k=1}^{M} \frac{1}{|J(\boldsymbol{f}_k^{-1}(\boldsymbol{C}_i))|} p_{ij}^k \right) q_j^n = \sum_{j=1}^{N} P_{ij} q_j^n \end{aligned}$$

we obtain the relation between the deterministic forward map $\boldsymbol{f}$ and the transition matrix of Eq. (2)

$$P_{ij} = \sum_{k=1}^{M} \frac{1}{|J(\boldsymbol{f}_k^{-1}(\boldsymbol{C}_i))|} p_{ij}^k\,.$$

If $M = 1$ for all i, p_{ij} coincides with the transpose of the adjoint of the transition matrix. At this point it is noted that the entries P_{ij} can be inferred from the statistics of the discretized dynamics or from available time series. By means of the above expression, the transition rates P_{ij} may then be used for our purpose of estimating the Jacobian, or any observable of interest that depends on it. For instance, we define, for $k > 1$,

$$A_i = \sum_{j=1}^{N} P_{ij} = \sum_{k=1}^{M} \frac{1}{|J(\boldsymbol{f}_k^{-1}(\boldsymbol{C}_i))|} \sum_{j=1}^{N} p_{ij}^k = \sum_{k=1}^{M} \frac{1}{|J(\boldsymbol{f}_k^{-1}(\boldsymbol{C}_i))|}\,, \tag{8}$$

where we used Eq. (6) in the last identity.

Let $k^*(i,j)$ be the index of the largest entry of p_{ij}^k for given i,j. We can then write:

$$\begin{aligned} B_j &= \max_i P_{ij} = \max_i \sum_{k=1}^{M} \frac{1}{|J(\boldsymbol{f}_k^{-1}(\boldsymbol{C}_i))|} p_{ij}^k \\ &\approx \max_i \sum_{k=1}^{M} \frac{1}{|J(\boldsymbol{C}_j)|} p_{ij}^k \approx \frac{1}{|J(\boldsymbol{C}_j)|} \max_i p_{ij}^{k^*(i,j)} \le \frac{1}{|J(\boldsymbol{C}_j)|}\,, \end{aligned}$$

where we approximated with $\boldsymbol{C}_j$ all the preimages of $\boldsymbol{C}_i$ falling in $\boldsymbol{X}_j$ and we used Eq. (7). Furthermore, since B_j is bounded by probability bound Eq. (3), we have that

$$B_j = \max_i P_{ij} \le \min\{|J(\boldsymbol{C}_j)|^{-1}, 1\}\,. \tag{9}$$

For an alternative derivation of the expressions for A_i and B_j, see Appendix.

The Perron–Frobenius operator $\mathcal{P}$ is often characterized as a contraction, satisfying $\|\mathcal{P}\rho\| \le \|\rho\|$. Thus, A_i defined in Eq. (8) can be viewed as the local inverse dissipation rate of the state-space volume centered at $\boldsymbol{C}_i$. In one dimension, B_j defined in Eq. (9) is an upper bound on the derivative of the forward map.

An addition of noise to each $\boldsymbol{x}$ does not alter A_i (Eq. (8)) because each p_{ij}^k remains normalized. However, noise increases the variance of p_{ij}^k, thereby reducing its maximal values. In regions where $\boldsymbol{f}^{-1}$ contracts the state space, $p_{ij}^k \approx 1$ are weakly affected if the noise remains small compared to the control volumes. Consequently, certain entries B_j (Eq. (9)) will stay close to $1/|J(\boldsymbol{C}_j)|$, allowing for the extraction of the Jacobian.

The expressions for A_i and B_j represent a novel quantitative relationship between the transition matrix and the local Jacobian determinant. This relationship allows us to estimate dissipation and instability fields directly from observed dynamics without requiring knowledge of the underlying equations. To our knowledge, this connection between statistical descriptions of dynamics (via the transition matrix) and local properties of the underlying map (via the Jacobian) is a novel contribution to dynamical systems theory.

3. Jacobian of chaotic maps

In this section, we apply the method described above to a variety of one-dimensional and two-dimensional dynamical systems. Our primary objective is to relate the entries of the numerically estimated transfer operator to the Jacobian of the underlying system. It is important to emphasize that, while our examples utilize known maps for validation purposes, our methodology is fundamentally data-driven and does not require knowledge of the governing equations. In particular, the expressions obtained in this section for the observables A_i and B_j (upper bound) are to be considered ground truth to test their respective estimates from Eqs. (8) and (9) from the transition matrix P_{ij}.

3.1. One-dimensional chaotic maps

For detailed discussions of the dynamical systems that follow, the reader is referred to Chapter 17 of [53].

3.1.1. The Ulam map

The mapping

$$x_{n+1} = 1 - 2(x_n)^2,$$

on the interval $x_n \in (-1,1]$ for all n is known as 'Ulam map'. The Perron–Frobenius evolution equation for the probability density is

$$\rho^{n+1}(C_i) = \frac{1}{4}\left(\frac{2}{1-C_i}\right)^{\frac{1}{2}} \left[\rho^n\left(\left(\frac{1-C_i}{2}\right)^{\frac{1}{2}} \right) + \rho^n\left(-\left(\frac{1-C_i}{2}\right)^{\frac{1}{2}} \right) \right],$$

and, subsequently,

$$A_i = \sum_k \frac{1}{|J(f_k^{-1}(C_i))|} = \frac{\sqrt{2}}{2}\left(\frac{1}{1-C_i}\right)^{\frac{1}{2}}, \tag{10}$$

with

$$B_j \le \frac{1}{|J(C_j)|} = \frac{1}{4|C_j|}\,. \tag{11}$$

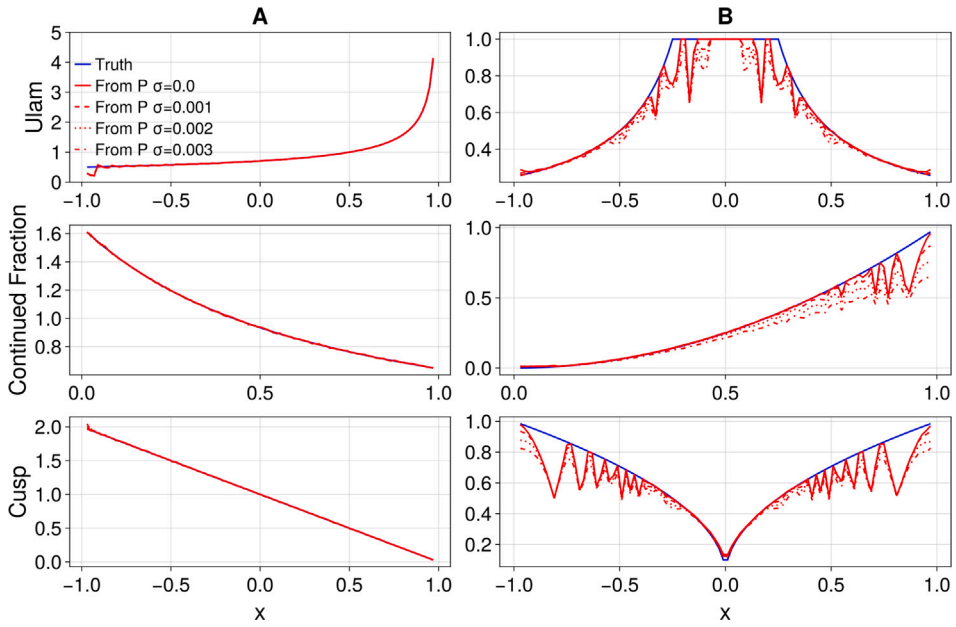

Fig. 1. *Ulam, continued fraction and cusp maps:* Plots of A_i and B_j (left and right column, respectively) derived from the transition matrix (depicted with red lines), along with their analytical estimates (shown in blue), for the Ulam, continued fraction, and cusp maps. Noise amplitudes of $\sigma = 0, 0.001, 0.002, 0.003$ have been applied to the maps.

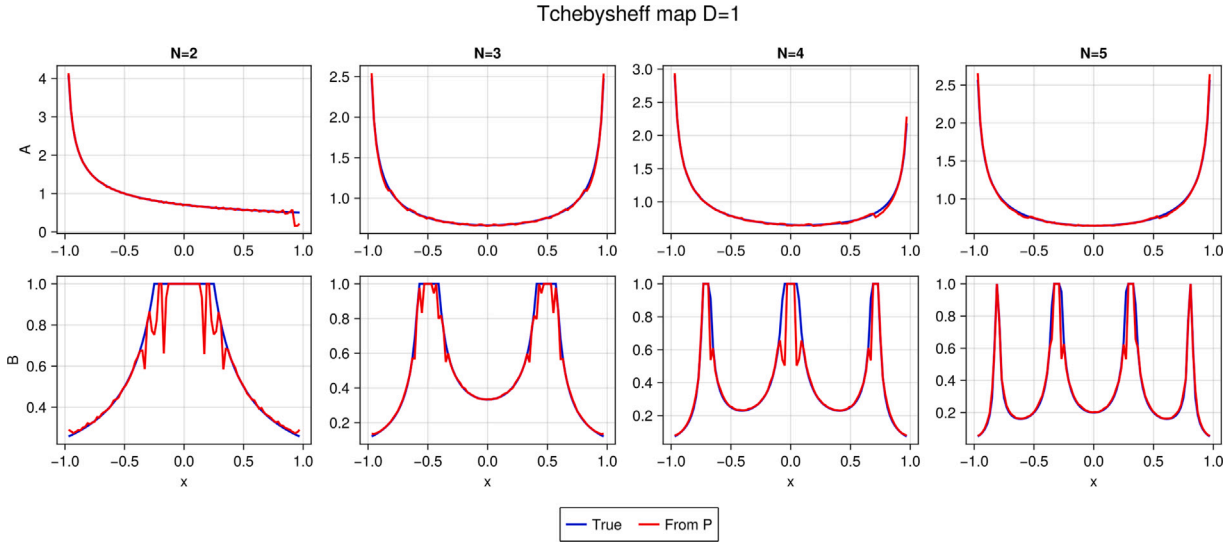

Fig. 2. *One-dimensional Chebyshev map:* Plots of A_i and B_j derived from the transition matrix (red lines), along with their analytical estimates (blue lines), for the Chebyshev map defined in Eq. (16) with $N = 2, 3, 4,$ and 5, and $\sigma = 0$.

3.1.2. Continued fraction map

In the case of the continued fraction map, given by

$$f(x) = \frac{1}{x} - \left\lfloor \frac{1}{x} \right\rfloor, \qquad x_n \in [0,1] \quad \forall n,$$

we have

$$\rho^{n+1}(C_i) = \sum_{k=1}^{\infty} \frac{1}{(k+C_i)^2} \rho^n\left(\frac{1}{C_i+k}\right),$$

$$A_i = \sum_k \frac{1}{|J(f_k^{-1}(C_i))|} = \Psi(1+C_i), \tag{12}$$

and

$$B_j \le \frac{1}{|J(C_j)|} = C_j^2, \tag{13}$$

where $\Psi(x) = \frac{\Gamma'(x)}{\Gamma(x)}$ is the polygamma function (logarithmic derivative of the Gamma function), and $\lfloor x \rfloor$ denotes the integer part of x.

3.1.3. Cusp map

The map

$$f(x) = 1 - 2|x|^{\frac{1}{2}}, \qquad x_n \in [-1,1] \quad \forall n$$

is known as the 'cusp map', with the Perron–Frobenius evolution equation for the probability density

$$\rho^{n+1}(C_i) = \frac{1-C_i}{2}\left[\rho^n\left(\frac{(1-C_i)^2}{4}\right) + \rho^n\left(-\frac{(1-C_i)^2}{2}\right)\right],$$

$$A_i = \sum_k \frac{1}{|J(f_k^{-1}(C_i))|} = 1 - C_i, \tag{14}$$

and

$$B_j \le \frac{1}{|J(C_j)|} = \sqrt{|C_j|}. \tag{15}$$

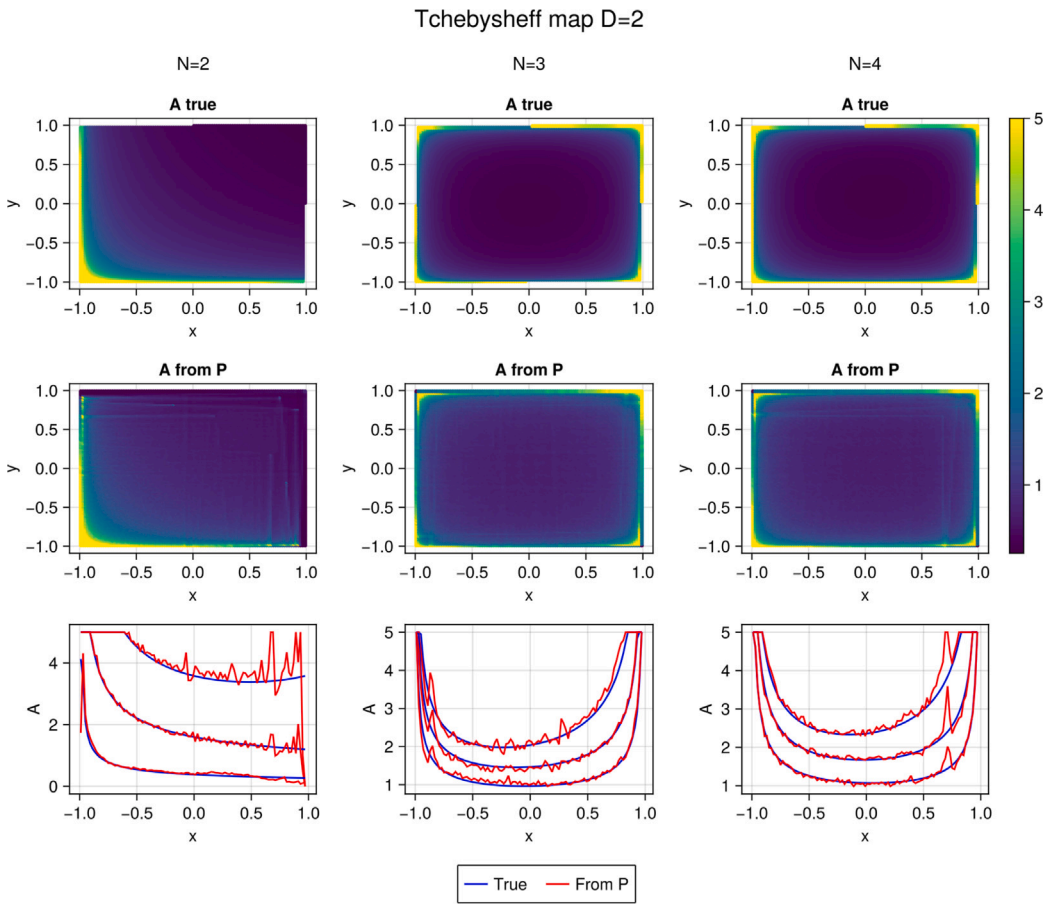

Fig. 3. *Two-dimensional coupled Chebyshev map.* Heat maps and scatter plots comparing the A_i values from the transition matrix with their analytical counterparts for the map in Eq. (19), using $N = 2, 3, 4$ and coupling parameter $a = 0.01$. Below the heatmaps, we compare A_i as a function of the x coordinate for different values of y ($y = -0.98, -0.9, 0.8$ for $N = 2$ and $y = -0.98, -0.96, 0.8$ for $N = 3, 4$), obtained through the two different methods.

3.1.4. One-dimensional Chebyshev map

The one-dimensional Chebyshev map is defined as:

$$x_{n+1} = T_N(x_n), \qquad x \in [-1, 1], \tag{16}$$

where $T_N(x)$ is the Nth Chebyshev polynomial $T_N(x) = \cos(N \arccos(x))$. The Perron–Frobenius evolution equation for this map yields

$$A_i = \sum_{k=0}^{N-1} \frac{1}{|J(f_k^{-1}(C_i))|} = \sum_{k=0}^{N-1} \frac{\sqrt{1 - x_k^2(C_i)}}{N \left|\sin(N \arccos(x_k(C_i)))\right|}, \tag{17}$$

and

$$B_j \le \frac{1}{|J(C_j)|} = \frac{\sqrt{1 - C_j^2}}{N \left|\sin(N \arccos(C_j))\right|}, \tag{18}$$

where

$$x_k(C_i) = \cos\left(\frac{\arccos(C_i) + 2\pi k}{N}\right), \quad k = 0, 1, \ldots, N-1.$$

3.1.5. Results

We partition the state space into $N = 100$ equally sized control volumes, and assign every orbit point to its corresponding volume. Using this cluster of trajectories, we construct the transition matrix $\boldsymbol{P}$, from which we extract our estimates for the inverse dissipation $A_i = \sum_{j=1}^{N} P_{ij}$ and the local instability rate $B_j = \max_i P_{ij}$ from the data collected by running the dynamics. We also repeat the procedure with additive Gaussian white noise of amplitude σ.

In (Fig. 1, 2) we compare the expressions A_i and B_j obtained from the transition matrix with their analytical values, as defined in Eqs. (10) to (17). In the panels representing B_j we set to unity all values of the analytical estimate of B_j larger than one, since the elements of B_j obtained from the transition matrix cannot be larger than unity.

Upon varying the noise amplitudes in Fig. 1, we observe a consistent pattern: the 'data' estimate of A_i accurately reproduces its expected value, without appreciable deviations, up to the precision of our numerics, with or without additive noise. On the other hand, the data estimate of B_j is less accurate, as well as more sensitive to noise. In particular, the local instability rate is often underestimated as the noise amplitude increases. However, the quality of the estimates of B_j does follow a pattern that depends on the instability itself: it is in fact noted from the plots that the estimate for the instability rate B_j is consistently the more accurate and noise-robust, the larger the Jacobian, or equivalently, the smaller B_j.

3.2. Two-dimensional coupled Chebyshev maps

This section demonstrates the application of the proposed methodology to estimate the Jacobian for two-dimensional coupled Chebyshev maps [54]. We will compute coefficients A_i and B_j for small coupling strengths and polynomial orders $N = 2, 3, 4$.

The two-dimensional coupled Chebyshev map is defined by:

$$\begin{aligned} x_{n+1} &= (1-a)\, T_N(x_n) + a\, T_N(y_n), \\ y_{n+1} &= (1-a)\, T_N(y_n) + a\, T_N(x_n), \end{aligned} \tag{19}$$

where $T_N(\cdot)$ is the Nth Chebyshev polynomial, and the parameter $a \in [0, 1]$ controls the coupling strength. For the particular cases $N = 2, 3, 4$, the polynomials are

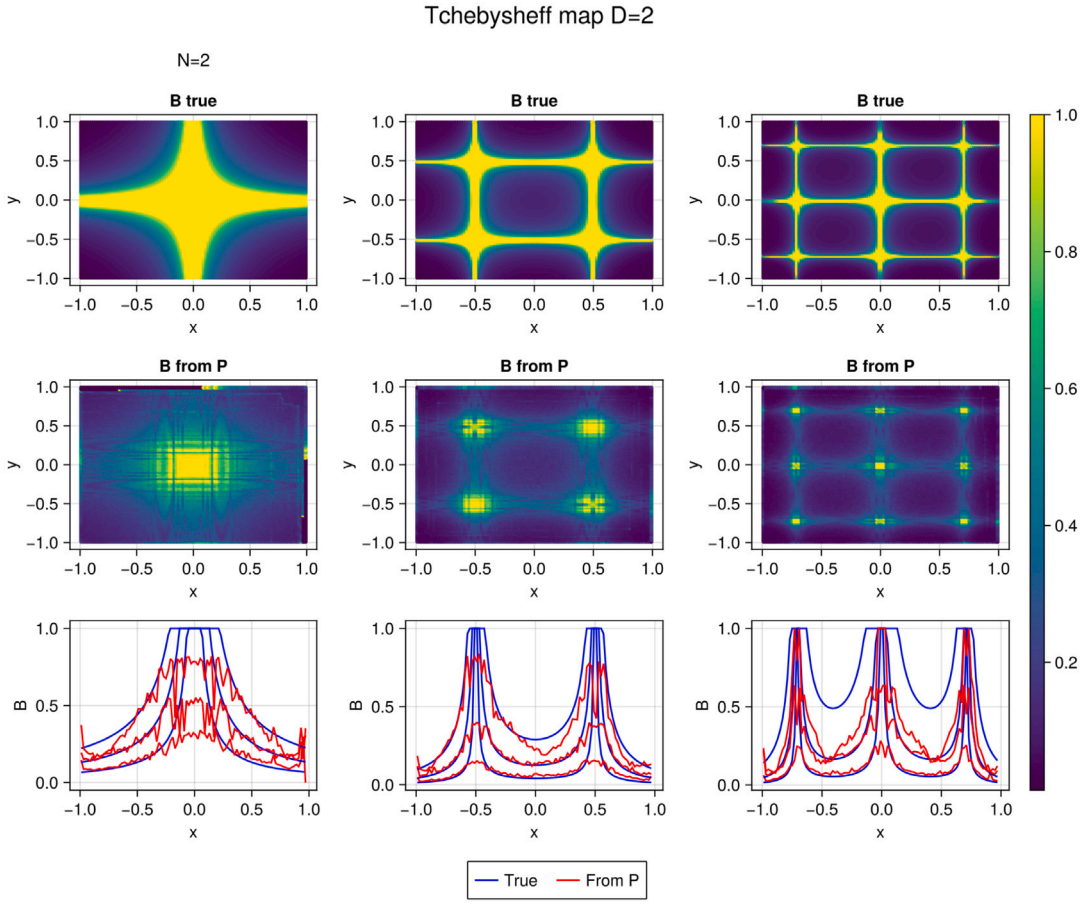

Fig. 4. *Two-dimensional coupled Chebyshev map.* Same as Fig. 3, but for B_j. The values of y used in the plots in the last row are $y = -0.98, -0.5, -0.3$ for $N = 2$, $y = -0.98, -0.7, -0.4$ for $N = 3$ and $y = -0.4, -0.1, -0.04$ for $N = 4$.

- $T_2(x) = 2x^2 - 1$,
- $T_3(x) = 4x^3 - 3x$,
- $T_4(x) = 8x^4 - 8x^2 + 1$.

Coupled Chebyshev maps with a relatively weak coupling (here the parameter a is set to 0.01 throughout the simulations presented) are ergodic and mixing like their uncoupled counterparts, yet they exhibit multidimensional features (e.g. their natural measure), whereas they tend to develop coherent structures and synchronization for stronger couplings [55]. Moreover, still in the regime of weak coupling, the dynamics is locally expanding (both eigendirections are unstable), rather than hyperbolic (only one is unstable) [54], which yields non-trivial dissipation and instability fields in the state space. For that reason in particular, the local Jacobian is still a measure of instability, and so is our observable B_j.

The Jacobian of the forward map in Eq. (19) is:

$$|J(x,y)| \;=\; \Big|(1-a)^2\,T_N'(x)\,T_N'(y) \;-\; a^2\,T_N'(y)\,T_N'(x)\Big|,$$

where

$$T_N'(x) \;=\; \frac{-N\,\sin\big(N\,\arccos(x)\big)}{\sqrt{1-x^2}}.$$

Although the inverse of the two-dimensional map does not admit a closed-form solution for arbitrary N, it can be determined analytically for $N = 2$:

$$x_n \;=\; \pm\sqrt{\frac{-1 - x_{n+1} + a\,(2 + x_{n+1} + y_{n+1})}{-2 + 4a}},$$

$$y_n \;=\; \pm\sqrt{\frac{-1 - y_{n+1} + a\,(2 + x_{n+1} + y_{n+1})}{-2 + 4a}},$$

and $N = 4$:

$$x_n \;=\; \pm\frac{1}{2}\sqrt{2 \pm \sqrt{\frac{-2\,(1 + x_{n+1}) + 2a\,(2 + x_{n+1} + y_{n+1})}{-1 + 2a}}},$$

$$y_n \;=\; \pm\frac{1}{2}\sqrt{2 \pm \sqrt{\frac{-2\,(1 + y_{n+1}) + 2a\,(2 + x_{n+1} + y_{n+1})}{-1 + 2a}}}.$$

For T_3, the inverse map is given by the solution to the cubic equations:

$$(x_n)^3 \;-\; \tfrac{3}{4}\,x_n \;+\; \tfrac{a}{4(1-2a)}\,y_{n+1} \;+\; \tfrac{a-1}{4(1-2a)}\,x_{n+1} \;=\; 0,$$

$$(y_n)^3 \;-\; \tfrac{3}{4}\,y_n \;+\; \tfrac{a}{4(1-2a)}\,x_{n+1} \;+\; \tfrac{a-1}{4(1-2a)}\,y_{n+1} \;=\; 0.$$

We simulate the Chebyshev map over 10^7 time steps for $N = 2, 3, 4$, partitioning the state space into a 100×100 grid of equally size control volumes to construct the transition matrix. (Fig. 3, 4) present the results for $N = 2, 3, 4$, comparing the numerical estimates of A_i, B_j with their analytical counterparts. Similar observations to those made in previous examples apply here. Specifically, we observe that A_i closely matches its analytical expectation across the state space. In contrast, the observable B_j computed from data is accurate primarily in the more unstable regions of the state space, while it provides poorer estimates of the inverse of the Jacobian in the dynamically less unstable or nearly marginal regions.

4. Conclusions

In this study, we have established a novel methodology for extracting information about the Jacobian determinant directly from the transition matrix of a discretized Perron–Frobenius operator. Our primary contribution is the demonstration that local dissipation and instability fields are intrinsically encoded in this matrix. This provides a new pathway to connect the global statistical features of a dynamical system with its local dynamics.

The numerical simulations of both one-dimensional and two-dimen sional chaotic maps demonstrate the robustness of our methodology – but also highlight specific challenges. In particular, in the two-dimensional case, we observe that state-space regions, where the local Jacobian is accurately reproduced by the data-determined observable B, are bounded.

One potential approach we aim to explore in the future involves synthesizing the less accurate information from the estimate B for the local Jacobian, with the more precise data from the observable A for the dissipation. This strategy would involve initially using B to aid in the estimation of the deterministic flow/map $\boldsymbol{f}$. Subsequently, the inverse function $\boldsymbol{f}^{-1}$ could be calculated, allowing us to verify the accuracy of our estimation. This verification would be accomplished by using $\boldsymbol{f}^{-1}$ to estimate the dissipation A, followed by a matching of this result to A, this time as derived from the transition matrix via Eq. (8). This hybridized approach may help overcome the limitations associated with using the observable B alone for the reconstruction of the Jacobian.

Another challenge can arise from errors in determining the entries of the transition matrix corresponding to regions of coordinate space that are rarely visited by the dynamical system, a common occurrence when only a limited amount of data is available. This introduces noise into both observables A and B. The resulting effects are more pronounced in B, since each entry corresponds directly to an individual entry from the transition matrix, unlike A, where each entry is a sum of all the elements in each column, effectively averaging out the noise introduced by the finite amount of processed data.

To address these limitations, a key future direction is to enhance the estimation of the transition matrix itself. The Ulam method, which we have used here, is fundamentally a histogram-based estimator. As shown in [56], using more advanced techniques such as kernel density estimation (KDE) can yield a more statistically consistent and smoother approximation of the Perron–Frobenius operator. Adopting a KDE-based framework for constructing the transition matrix is expected to be beneficial for the evaluation of the Jacobian determinant, as it can mitigate the bias inherent in piecewise-constant histogram methods and provide a more accurate representation of the underlying probability densities, especially with sparse data. Furthermore, a thorough comparison of our proposed methodology with the classical k-nearest neighbors approach is essential. A systematic study, evaluating computational efficiency and robustness to noise for both methods under various conditions, will be conducted to clarify the relative advantages and establish the viability of the Perron–Frobenius based approach in the broader context of data-driven dynamical systems analysis.

In summary, the methodology developed in this study provides a new pathway to connect statistical features of dynamical systems, specifically the transition matrix, with the local dynamics captured by the Jacobian. While our approach shows promise in effectively reconstructing the Jacobian from observed data, it also highlights challenges, particularly in higher-dimensional systems where the relationship between the transition matrix and the Jacobian becomes less straightforward. Future research will focus on refining the approach by combining the insights from both observables A and B to improve the accuracy and reliability of the Jacobian reconstruction. Additionally, expanding this methodology to handle more complex dynamical systems and exploring the effects of noise and other perturbations will be crucial for broadening the applicability of this approach and for demonstrating its potential.

CRediT authorship contribution statement

Ludovico T. Giorgini: Writing – review & editing, Writing – original draft, Visualization, Validation, Supervision, Software, Resources, Project administration, Methodology, Investigation, Funding acquisition, Formal analysis, Data curation, Conceptualization. **Andre N. Souza:** Writing – review & editing, Writing – original draft, Visualization, Validation, Supervision, Software, Resources, Project administration, Methodology, Investigation, Funding acquisition, Formal analysis, Data curation, Conceptualization. **Domenico Lippolis:** Writing – review & editing, Writing – original draft, Visualization, Validation, Supervision, Software, Resources, Project administration, Methodology, Investigation, Funding acquisition, Formal analysis, Data curation, Conceptualization. **Predrag Cvitanović:** Writing – review & editing, Writing – original draft, Visualization, Validation, Supervision, Software, Resources, Project administration, Methodology, Investigation, Funding acquisition, Formal analysis, Data curation, Conceptualization. **Peter Schmid:** Writing – review & editing, Writing – original draft, Visualization, Validation, Supervision, Software, Resources, Project administration, Methodology, Investigation, Funding acquisition, Formal analysis, Data curation, Conceptualization.

Declaration of competing interest

The authors declare that they have no known competing financial interests or personal relationships that could have appeared to influence the work reported in this paper.

Acknowledgments

The authors want to thank the 2022 Geophysical Fluid Dynamics Program, where a significant portion of this research was undertaken; the GFD Program is supported by the National Science Foundation, United States Grant No. 1829864, United States and the Office of Naval Research, United States. We are grateful to Edward A. Spiegel for his unwavering support through the Woods Hole GFD turbulent summers that begot this collaboration. LTG was supported by the Swedish Research Council (Vetenskapsradet) Grant No. 638-2013-9243. AS acknowledges support by Schmidt Sciences, LLC, through the Bringing Computation to the Climate Challenge, an MIT Climate Grand Challenge Project.

Appendix. Alternative derivation of the expressions for A_i and B_j

Let us write a density in the state space as a sum of contributions over the discretization Eq. (1), $\boldsymbol{X} = [\boldsymbol{X}_1, \ldots, \boldsymbol{X}_N]$,

$$\rho^n(\boldsymbol{x}) = \sum_j \alpha_j^n \rho_j(\boldsymbol{x}), \tag{20}$$

where the ρ_j's are smooth functions peaked at the centroid $\boldsymbol{C}_j$ of each interval, for example the Gaussians

$$\rho_j(\boldsymbol{x}) = \frac{1}{(2\pi\sigma^2)^{D/2}} \exp\left(-\frac{\|\boldsymbol{x}-\boldsymbol{C}_j\|^2}{2\sigma^2}\right).$$

We set $\sigma^2 = [\Omega/N]^{2/D}/2\pi$ to ensure that the support of ρ_j approximately coincides with $\boldsymbol{X}_j$, thereby rendering the Gaussian basis nearly orthogonal. Consequently, we can write:

$$q_i^n = \int_{\boldsymbol{X}_i} \rho^n(\boldsymbol{x})\, d\boldsymbol{x} \approx \alpha_i^n.$$

The evolution of the probability of each interval reads

$$q_i^{n+1} = \int_{\boldsymbol{X}_i} \rho^{n+1}(\boldsymbol{x}) d\boldsymbol{x} = \int_{\boldsymbol{X}_i} d\boldsymbol{x} \int_{\boldsymbol{X}} d\boldsymbol{y}\, \delta(\boldsymbol{x}-\boldsymbol{f}(\boldsymbol{y}))\rho^n(\boldsymbol{y})$$

where the Perron–Frobenius operator $\int_{\boldsymbol{X}} d\boldsymbol{y}\,\delta(x-\boldsymbol{f}(y))\cdot$ transports state-space densities forward in time. Using the partition (20), the previous is rewritten as

$$\begin{aligned} q_i^{n+1} &= \sum_{j=1}^{N} \alpha_j^n \int_{\boldsymbol{X}_i} d\boldsymbol{x} \int_{\boldsymbol{X}} d\boldsymbol{y}\delta(\boldsymbol{x}-\boldsymbol{f}(\boldsymbol{y}))\rho_j(\boldsymbol{x}) \\ &\approx \sum_{j=1}^{N} q_j^n \int_{\boldsymbol{X}_i} d\boldsymbol{x} \int_{\boldsymbol{X}_j} d\boldsymbol{y}\delta(\boldsymbol{x}-\boldsymbol{f}(\boldsymbol{y}))\rho_j(\boldsymbol{x}) \\ &= \sum_{j=1}^{N} q_j^n \sum_{k=1}^{M} \int_{\boldsymbol{X}_i} d\boldsymbol{x} \frac{\rho_j(\boldsymbol{f}_k^{-1}(\boldsymbol{x}))}{|J(\boldsymbol{f}_k^{-1}(\boldsymbol{x}))|}\,. \end{aligned} \tag{21}$$

Now suppose that the partition $\boldsymbol{X}$ is sufficiently fine for the integrals to be well approximated by the value of the integrand at the centroid $\boldsymbol{C}_i$ of $\boldsymbol{X}_i$ times the measure of the interval. Recalling that the ρ_j's are Gaussians, we write

$$q_i^{n+1} \simeq \sum_{j=1}^{N} q_j^n \sum_{k=1}^{M} \frac{e^{-\|\boldsymbol{f}_k^{-1}(\boldsymbol{C}_i)-\boldsymbol{C}_j\|^2/2\sigma^2}}{|J(\boldsymbol{f}_k^{-1}(\boldsymbol{C}_i))|}\,, \tag{22}$$

having chosen $\sigma^2 = [\mu(\boldsymbol{X}_i)]^{2/D}/2\pi$ for the normalization to be unity. One can then approximately identify the entries of the transition matrix with

$$P_{ij} \simeq \sum_{k=1}^{M} \frac{e^{-\|\boldsymbol{f}_k^{-1}(\boldsymbol{C}_i)-\boldsymbol{C}_j\|^2/2\sigma^2}}{|J(\boldsymbol{f}_k^{-1}(\boldsymbol{C}_i))|}\,.$$

The probabilities P_{ij} to go from $\boldsymbol{X}_j$ to $\boldsymbol{X}_i$ in one iteration of the transfer operator are constrained by the condition

$$\sum_{i}^{N} P_{ij} = 1\,,$$

so that

$$\sum_{i=1}^{N}\sum_{k=1}^{M} \frac{e^{-\|\boldsymbol{f}_k^{-1}(\boldsymbol{C}_i)-\boldsymbol{C}_j\|^2/2\sigma^2}}{|J(\boldsymbol{f}_k^{-1}(\boldsymbol{C}_i))|} \simeq 1\,,$$

and, as every single $i-$th contribution is positive definite, we have

$$\sum_{k=1}^{M} \frac{e^{-\|\boldsymbol{f}_k^{-1}(\boldsymbol{C}_i)-\boldsymbol{C}_j\|^2/2\sigma^2}}{|J(\boldsymbol{f}_k^{-1}(\boldsymbol{C}_i))|} \lesssim 1\,.$$

The largest entries of the transfer matrix are realized when $\boldsymbol{X}_j$ maps into $\boldsymbol{X}_i$, that is for a special k^* such that $\|\boldsymbol{f}_{k^*}^{-1}(\boldsymbol{C}_i)-\boldsymbol{C}_j\|^2 < \sigma^2$, and so we have rederived Eq. (9),

$$B_j \equiv \max_i P_{ij} \simeq \frac{1}{|J(\boldsymbol{f}_{k^*}^{-1}(\boldsymbol{C}_i))|} \approx \frac{1}{|J(\boldsymbol{C}_j)|}\,. \tag{23}$$

All the previous expressions from (22) up to (23) rely on the assumption of non-vanishing Jacobians $|J(\boldsymbol{f}_{k^*}^{-1}(\boldsymbol{C}_i))|$ and $|J(\boldsymbol{C}_j)|$. If, instead, the Jacobian does vanish somewhere in the intervals $\boldsymbol{X}_i$ or $\boldsymbol{X}_j$, the approximation (22) no longer holds, and

$$\int_{\boldsymbol{X}_i} d\boldsymbol{x} \frac{\rho_j^n(\boldsymbol{f}_k^{-1}(\boldsymbol{x}))}{|J(\boldsymbol{f}_k^{-1}(\boldsymbol{x}))|} = \int_{\boldsymbol{f}_k^{-1}(\boldsymbol{X}_i)} d\boldsymbol{y}\,\rho_j^n(\boldsymbol{y})$$

$$= \int_{\boldsymbol{f}_k^{-1}(\boldsymbol{X}_i)} \frac{d\boldsymbol{y}}{(2\pi\sigma^2)^{D/2}} e^{-\|\boldsymbol{y}-\boldsymbol{C}_j\|^2/2\sigma^2} \le 1$$

now provides an upper bound for $\max_i P_{ij}$. On the other hand, the sum of the probabilities of landing in $\boldsymbol{X}_i$ is, confirming Eq. (8),

$$A_i \equiv \sum_j P_{ij} \simeq \sum_{j=1}^{N}\sum_{k=1}^{M} \frac{e^{-\|\boldsymbol{f}_k^{-1}(\boldsymbol{C}_i)-\boldsymbol{C}_j\|^2/2\sigma^2}}{|J(\boldsymbol{f}_k^{-1}(\boldsymbol{C}_i))|} \approx \sum_{k=1}^{M} \frac{1}{|J(\boldsymbol{f}_k^{-1}(\boldsymbol{C}_i))|}\,,$$

estimating that the only non-negligible contributions to the sum over j are coming from the $\boldsymbol{C}_j$'s such that $\|\boldsymbol{f}_k^{-1}(\boldsymbol{C}_i)-\boldsymbol{C}_j\| < \sigma^2$.

Data availability

Data will be made available on request.

References

[1] F. Lejarza, M. Baldea, Data-driven discovery of the governing equations of dynamical systems via moving horizon optimization, Sci. Rep. 12 (1) (2022) 11836.

[2] P. Holmes, J.L. Lumley, G. Berkooz, Turbulence, Coherent Structures, Dynamical Systems and Symmetry, Cambridge University Press, 2012.

[3] S.L. Brunton, J.L. Proctor, J.N. Kutz, Discovering governing equations from data: Sparse identification of nonlinear dynamical systems, Proc. Natl. Acad. Sci. 113 (15) (2016) 3932–3937.

[4] P.J. Schmid, Dynamic mode decomposition of numerical and experimental data, J. Fluid Mech. 656 (2010) 5–28.

[5] M. Santos Gutiérrez, V. Lucarini, M.D. Chekroun, M. Ghil, Reduced-order models for coupled dynamical systems: Data-driven methods and the Koopman operator, Chaos: An Interdiscip. J. Nonlinear Sci. 31 (5) (2021).

[6] A.J. Chorin, P. Stinis, Problem reduction, renormalization, and memory, Commun. Appl. Math. Comput. Sci. 1 (1) (2007) 1–27.

[7] J. Moehlis, T.R. Smith, P. Holmes, H. Faisst, Models for turbulent plane Couette flow using the proper orthogonal decomposition, Phys. Fluids 16 (6) (2004) 2011–2024.

[8] H. Kantz, T. Schreiber, Nonlinear Time Series Analysis, Cambridge University Press, 2004.

[9] L.T. Giorgini, S.H. Lim, W. Moon, J.S. Wettlaufer, Precursors to rare events in stochastic resonance, Europhys. Lett. 129 (4) (2020) 40003.

[10] S.H. Lim, L.T. Giorgini, W. Moon, J.S. Wettlaufer, Predicting critical transitions in multiscale dynamical systems using reservoir computing, Chaos: An Interdiscip. J. Nonlinear Sci. 30 (123126) (2020).

[11] L.T. Giorgini, Data-driven decomposition of conservative and non-conservative dynamics in multiscale systems, 2025, arXiv preprint arXiv:2505.01895.

[12] E.N. Lorenz, Deterministic nonperiodic flow, J. Atmos. Sci. 20 (2) (1963) 130–141.

[13] T. Schneider, S. Lan, A. Stuart, J. Teixeira, Earth system modeling 2.0: A blueprint for models that learn from observations and targeted high-resolution simulations, Geophys. Res. Lett. 44 (24) (2017) 12–396.

[14] L.T. Giorgini, W. Moon, N. Chen, J.S. Wettlaufer, Non-Gaussian stochastic dynamical model for the El Niño Southern Oscillation, Phys. Rev. Res. 4 (2) (2022) L022065.

[15] L.T. Giorgini, S.H. Lim, W. Moon, N. Chen, J.S. Wettlaufer, Modeling the El Niño Southern Oscillation with neural differential equations, in: Proceedings of the 38th International Conference on Machine Learning, 2021, p. 19.

[16] T.N. Palmer, Predicting uncertainty in forecasts of weather and climate, Rep. Progr. Phys. 63 (2) (2000) 71–116.

[17] A.J. Majda, J. Harlim, Filtering Complex Turbulent Systems, Cambridge University Press, 2012.

[18] N. Keyes, L. Giorgini, J. Wettlaufer, Stochastic paleoclimatology: Modeling the EPICA ice core climate records, Chaos: An Interdiscip. J. Nonlinear Sci. 33 (9) (2023).

[19] M. Baldovin, F. Cecconi, A. Provenzale, A. Vulpiani, Extracting causation from millennial-scale climate fluctuations in the last 800 kyr, Sci. Rep. 12 (1) (2022) 15320.

[20] G. Vissio, V. Lucarini, A proof of concept for scale-adaptive parametrizations: The case of the Lorenz'96 model, Q. J. R. Meteorol. Soc. 144 (710) (2018) 63–75.

[21] L.T. Giorgini, K. Deck, T. Bischoff, A. Souza, Response theory via generative score modeling, Phys. Rev. Lett. 133 (2024) 267302, http://dx.doi.org/10.1103/PhysRevLett.133.267302.

[22] L.T. Giorgini, F. Falasca, A.N. Souza, Predicting forced responses of probability distributions via the fluctuation-dissipation theorem and generative modeling, 2025, arXiv preprint arXiv:2504.13333.

[23] F. Black, M. Scholes, The pricing of options and corporate liabilities, J. Political Econ. 81 (3) (1973) 637–654.

[24] A.J. Lotka, Elements of physical biology, Science 61 (1576) (1925) 400–405.

[25] S.H. Strogatz, Nonlinear Dynamics and Chaos: With Applications to Physics, Biology, Chemistry, and Engineering, Westview Press, 1994.

[26] P. Cvitanović, R. Artuso, R. Mainieri, G. Tanner, G. Vattay, N. Whelan, A. Wirzba, Chaos: Classical and Qantum, Niels Bohr Inst., Copenhagen, 2025, URL https://ChaosBook.org.

[27] A. Vulpiani, Chaos: From Simple Models to Complex Systems, World Scientific, 2010.

[28] A.N. Souza, T. Lutz, G.R. Flierl, Statistical non-locality of dynamically coherent structures, J. Fluid Mech. 966 (2023) A44.

[29] G. Geogdzhayev, A.N. Souza, R. Ferrari, The evolving butterfly: Statistics in a changing attractor, Phys. D: Nonlinear Phenom. (2024) 134107.

[30] L.T. Giorgini, A.N. Souza, P.J. Schmid, Reduced Markovian models of dynamical systems, 2023, https://arXiv.org/abs/2308.10864.

[31] A.N. Souza, Representing turbulent statistics with partitions of state space. Part 1. Theory and methodology, J. Fluid Mech. 997 (2024) A1, http://dx.doi.org/10.1017/jfm.2024.658.

[32] A.N. Souza, Representing turbulent statistics with partitions of state space. Part 2. The compressible Euler equations, J. Fluid Mech. 997 (2024) A2, http://dx.doi.org/10.1017/jfm.2024.657.

[33] A.N. Souza, S. Silvestri, A modified bisecting K-means for approximating transfer operators: Application to the Lorenz equations, 2024, https://arXiv.org/abs/2412.03734.
[34] L.T. Giorgini, K. Deck, T. Bischoff, A. Souza, Response theory via generative score modeling, Phys. Rev. Lett. 133 (26) (2024) 267302.
[35] L.T. Giorgini, T. Bischoff, A.N. Souza, KGMM: A K-means clustering approach to Gaussian mixture modeling for score function estimation, 2025, arXiv preprint arXiv:2503.18054.
[36] J.-P. Eckmann, D. Ruelle, Ergodic theory of chaos and strange attractors, Rev. Modern Phys. 57 (3) (1985) 617–656, http://dx.doi.org/10.1103/RevModPhys.57.617.
[37] J.D. Farmer, J.J. Sidorowich, Predicting chaotic time series, Phys. Rev. Lett. 59 (8) (1987) 845–848, http://dx.doi.org/10.1103/PhysRevLett.59.845.
[38] M. Casdagli, Nonlinear prediction of chaotic time series, Phys. D: Nonlinear Phenom. 35 (3) (1989) 335–356, http://dx.doi.org/10.1016/0167-2789(89)90074-2.
[39] H.D.I. Abarbanel, R. Brown, J.J. Sidorowich, L.S. Tsimring, The analysis of observed chaotic data in physical systems, Rev. Modern Phys. 65 (4) (1993) 1331–1392, http://dx.doi.org/10.1103/RevModPhys.65.1331.
[40] M. Budišić, R. Mohr, I. Mezić, Applied Koopmanism, Chaos: An Interdiscip. J. Nonlinear Sci. 22 (2012) 047510.
[41] C. Zhang, H. Li, Y. Lan, Phase space partition with Koopman analysis, Chaos: An Interdiscip. J. Nonlinear Sci. 32 (2022) 063132.
[42] M. Buhl, M.B. Kennel, Statistically relaxing to generating partitions for observed time-series data, Phys. Rev. E 71 (2005) 046213.
[43] V. Lucarini, Interpretable and equation-free response theory for complex systems, 2025, arXiv preprint arXiv:2502.07908.
[44] M.D. Chekroun, N. Zagli, V. Lucarini, Kolmogorov modes and linear response of jump-diffusion models: Applications to stochastic excitation of the ENSO recharge oscillator, 2024, arXiv preprint arXiv:2411.14769.
[45] M. Asllani, J.D. Challenger, F.S. Pavone, L. Sacconi, D. Fanelli, The theory of pattern formation on directed networks, Nat. Commun. 5 (2014) 4517.
[46] M.L. Kringelbach, G. Deco, Brain states and transitions: Insights from computational neuroscience, Cell Rep. 32 (2020) 108128.
[47] P. Cvitanović, R. Artuso, L. Rondoni, E.A. Spiegel, Transporting densities, in: P. Cvitanović, R. Artuso, R. Mainieri, G. Tanner, G. Vattay (Eds.), Chaos: Classical and Quantum, Niels Bohr Inst., Copenhagen, 2025, p. 383, URL https://ChaosBook.org/paper.shtml#measure.
[48] D.J. Driebe, Fully Chaotic Maps and Time Reversal Symmetry, Springer, 1999.
[49] E. Ott, C. Grebogi, J.A. Yorke, Controlling chaos, Phys. Rev. Lett. 64 (11) (1990) 1196–1199.
[50] A. Wolf, J.B. Swift, H.L. Swinney, J.A. Vastano, Determining Lyapunov exponents from a time series, Phys. D: Nonlinear Phenom. 16 (3) (1985) 285–317.
[51] J.M.T. Thompson, H.B. Stewart, Nonlinear Dynamics and Chaos: Geometrical Methods for Scientists and Engineers, John Wiley and Sons, 2002.
[52] S. Wiggins, Introduction to Applied Nonlinear Dynamical Systems and Chaos, Springer, 2003.
[53] C. Beck, F. Schlögl, Y.L. Klimontovich, Thermodynamics of chaotic systems: An introduction, Phys.-Usp. 37 (7) (1994) 713.
[54] C. Dettmann, D. Lippolis, Periodic orbit theory of two coupled Tchebyscheff maps, Chaos Solitons Fractals 23 (1) (2005) 43–54, http://dx.doi.org/10.1016/j.chaos.2004.04.017.
[55] J. Yan, C. Beck, Information shift dynamics described by Tsallis $q = 3$ entropy on a compact phase space, Entropy 24 (2022) 1671, http://dx.doi.org/10.3390/e24111671.
[56] S. Surasinghe, J. Fish, E.M. Bollt, Learning transfer operators by kernel density estimation, Chaos: An Interdiscip. J. Nonlinear Sci. 34 (2) (2024) 023126, http://dx.doi.org/10.1063/5.0179937.